PHYSICS OF THE ALICE EXPERIMENT AT THE LHC

A.A. ISAYEV
Kharkov Institute of Physics and Technology, Academicheskaya Str. 1, Kharkov, 61108, Ukraine
Kharkov National University, Svobody Sq., 4, Kharkov, 61077, Ukraine

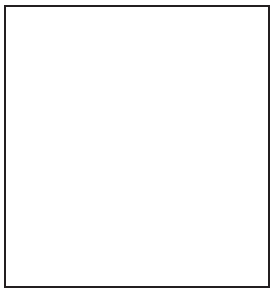

Some physical aspects of the ALICE experiment at the LHC are considered with emphasis on possible probes of quark-gluon plasma, created in ultrarelativistic heavy ion collisions.

1 Introduction

A Large Ion Collider Experiment (ALICE) [1,2] is the dedicated heavy ion experiment at the CERN Large Hadron Collider (LHC). The nucleon-nucleon center-of-mass energy for collisions of the heaviest ions at the LHC ($\sqrt{s} = 5.5\,\mathrm{TeV}$) will exceed that available at Relativistic Heavy Ion Collider (RHIC) in Brookhaven by a factor of about 30, opening up a new physics domain. ALICE will investigate equilibrium as well as non-equilibrium properties of strongly interacting matter in the energy density regime $\varepsilon \simeq 1 - 1000\,\mathrm{GeV\ fm}^{-3}$. At such huge energy densities a new state of matter, quark-gluon plasma (QGP), consisting of deconfined quarks and gluons, is expected to occur. ALICE is also aimed to investigate proton-proton, proton-nucleus collisions as well as collisions of lighter ions in order to get an important benchmark for collisions of heavy nuclei and to separate phenomena truly indicative of the hot and dense matter from other contributions. The focus of heavy ion physics is to study how collective phenomena in nuclear matter under conditions of extreme density and temperature emerge from the microscopic laws of elementary particle physics.

The quantum field theory of the strong nuclear force is Quantum Chromo-Dynamics (QCD). The color charge of quarks comes in three variants: red, green and blue. In particular, the gauge bosons - gluons, carry themselves a nonzero color charge, giving rise to the gluon self-interactions. The QCD Lagrangian reads

$$\mathcal{L} = \bar{q}(i\gamma^{\mu} D_{\mu} - \hat{m}_q)q - \frac{1}{4} F_{\mu\nu} F^{\mu\nu}, \tag{1}$$

where q and $\bar{q}$ denote the elementary matter fields, quarks and antiquarks. All flavor, color and spin indices in Eq. (1) are omitted. The mass matrix $\hat{m}_q = \mathrm{diag}(m_u, m_d, m_s, m_c, m_b, m_t)$ is the diagonal matrix in the flavor space, containing quark masses. The interaction of the quarks is encoded in the covariant derivative, $D_\mu = \partial_\mu - igA_\mu$, where A_μ denotes the gluon field, and the gauge coupling g quantifies the interaction strength. The gluons are massless particles with spin 1, carrying color charge in 8 different charge-anticharge combinations, e.g., red-antigreen, red-antiblue, etc. The commutator term in the gluon field tensor $F_{\mu\nu} = \partial_\mu A_\nu - \partial_\nu A_\mu + g[A_\mu, A_\nu]$ describes the gluon self-interactions.

The gluon self-interactions lead to a remarkable property of QCD, namely, the "anti-screening" of the color charge in the vacuum: the virtual quark-gluon cloud around a color charge in the polarized vacuum induces an increase of the effective charge with increasing distance. This property is closely related to the running coupling constant of QCD,

$$\alpha_s(Q) = \frac{12\pi}{(33 - 2n_f)\ln\frac{Q^2}{\Lambda^2}}, \tag{2}$$

n_f being the number of active quark flavors at the given momentum transfer Q (the number of flavors with $m_q \leq Q$), $\Lambda_{QCD} = 0.2\,\mathrm{GeV}$ being the regularization constant of QCD. Eq. (2) illustrates the property of asymptotic freedom: $\alpha_s \to 0$ as $Q \to \infty$ meaning that at small distances $r \sim 1/Q$ the quark and gluon interactions become weak and, hence, the perturbation theory on α_s can be developed. Oppositely, at scales $Q \sim \Lambda$, QCD becomes strongly coupled and perturbation theory cannot be used. In the strong coupling regime, new nonperturbative phenomena occur. Most notably, these are the confinement of color charges and the spontaneous breaking of chiral symmetry (SBCS). The former refers to the fact that quarks and gluons have never been observed as individual particles, but only come in "colorless" baryons, where three quarks carry an equal amount of three different color charges, or mesons, where quark and antiquark carry color charge and anticharge.

In the limit of vanishing bare quark masses, which is quite good approximation for the light up and down flavors, and, to a lesser extent, for the heavier strange flavor ($m_u \approx 5\,\mathrm{MeV}$, $m_d \approx 8\,\mathrm{MeV}$, and $m_s \approx 125\,\mathrm{MeV}$), the QCD Lagrangian is invariant under rotations of left-handed and right-handed quarks in isospin (flavor) space ($SU(3)_L \times SU(3)_R$ chiral symmetry of the QCD Lagrangian):

$$q_{L(R)} \longrightarrow e^{i\sum_a \xi^a_{L(R)}\lambda_a} q_{L(R)} \quad q_{L,R} = \frac{1}{2}(1 \mp \gamma_5)q, \tag{3}$$

where λ_a are the Gell-Mann matrices being the generators of $SU(3)$ group. However, the constituent quark mass (i.e., the mass of a bare quark dressed by a virtual quark-gluon cloud) breaks the chiral symmetry, because massive quarks can change their chirality so that it is no longer conserved. A physical reason for the origin of the constituent quark mass is that the QCD vacuum is not empty but filled with various condensates of quark-antiquark and gluon fields. As a consequence, the light quarks acquire an effective mass when propagate through the condensed vacuum, $m_q^* \simeq G\langle 0|\bar{q}q|0\rangle \simeq 0.4\,\mathrm{GeV}$ (G is the effective quark coupling constant), being larger than the bare quark masses by a factor of about 100. The theoretical understanding of the mechanisms underlying confinement and SBCS constitutes a major challenge in the contemporary particle and nuclear physics research.

2 QCD Phase Diagram

Lattice QCD (LQCD) provides a first-principles approach to studies of large-distance, nonperturbative aspects of QCD. The discrete space-time lattice that is introduced in this formulation of QCD is a regularization scheme particularly well suited for numerical calculations.

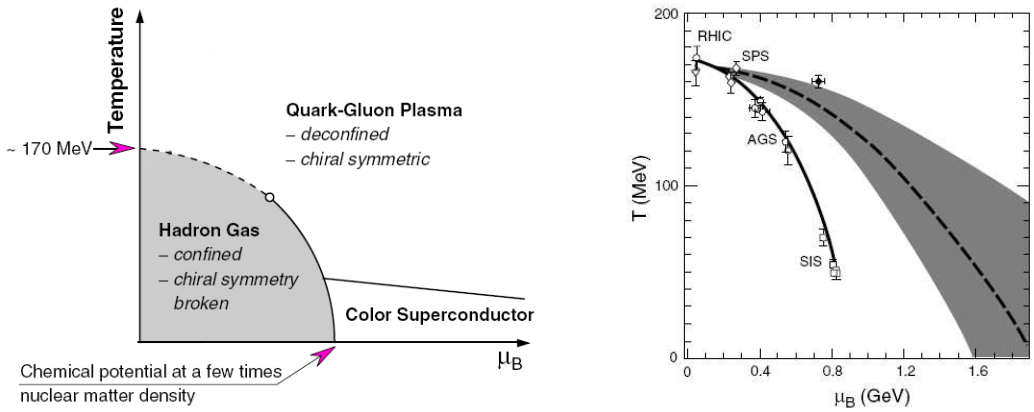

Figure 1: Left: Sketch of the QCD phase diagram. Right: LQCD results on the QCD-phase boundary (dashed line; the grey band indicates the uncertainty), shown together with the chemical freeze-out conditions for different experiments (open symbols); the filled point represents the endpoint of the crossover transition.

LQCD calculations predict that at the critical temperature $T_c \simeq 170\,\mathrm{MeV}$, corresponding to the energy density $\varepsilon_c \simeq 0.6\,\mathrm{GeV/fm^3}$, nuclear matter undergoes a phase transition to QGP. In QGP, chiral symmetry is approximately restored and quark masses are reduced from their large effective values in hadronic matter to their small bare ones. Since the heavy quarks (charm, bottom, top) are too heavy to play any role in the thermodynamics in the vicinity of the phase transition, the properties of 2-flavour or 3-flavour QCD are of a most interest. The order of the transition to QGP as well as the value of the critical temperature depend on the number of flavours and values of the quark masses. One finds $T_c = (175 \pm 15)\,\mathrm{MeV}$ in the chiral limit of 2-flavour QCD and a 20 MeV smaller value for 3-flavour QCD. First studies of QCD with two light quark flavours and a heavier (strange) quark flavour indicate that the transition temperature for the physically realized quark-mass spectrum is close to the 2-flavour value. Although the transition is of the second order in the chiral limit of 2-flavour QCD, and of the first order for 3-flavour QCD, it is likely to be only a rapid crossover in the case of the physically realized quark-mass spectrum [3]. The crossover, however, takes place in a narrow temperature interval around $T_c \simeq 170\,\mathrm{MeV}$ which makes the transition between the hadronic and plasma phases still well localized. The schematic representation of the QCD phase diagram in the plane "baryonic chemical potential - temperature" is shown in Fig. 1 (left) [1]. The dashed line indicates a possible region of the rapid crossover transition. The solid lines indicate likely first-order transitions. The open circle gives the second-order critical endpoint of the line of a first-order transition. At low temperature and low density, cold nuclear matter is a ground state of the system and at larger density the high density phase can be understood in terms of nearly degenerate, interacting Fermi gases of quarks. The remnant attractive interaction between quarks almost inevitably leads to quark-quark pairing and thus to the formation of a colour superconducting phase with $\langle 0|qq|0\rangle \neq 0$. All approximate model-based calculations suggest that the transition between cold nuclear matter and a color superconducting state is of the first order.

Fig. 1 (right) shows the results on determining the position of the phase boundary obtained in LQCD. The dashed line in this figure represents the extrapolation of the leading μ_B^2 order of the Taylor expansion of T_c to larger values of the chemical potential [4]. It is worth noting that, within the statistical uncertainties, the energy density along this line is constant and corresponds to $\varepsilon_c \simeq 0.6\,\mathrm{GeV/fm^3}$, i.e. to the same value as that found from lattice calculations at $\mu_B = 0$. It is thus conceivable that the QCD transition indeed sets in when the energy density reaches a certain critical value.

The pressure and energy density in QCD with 0, 2 and 3 degenerate quark flavours as well as with two light (up and down) flavours and a heavier (strange) quark flavour are shown in Fig. 2. It is seen that near the crossover temperature the energy density rapidly increases.

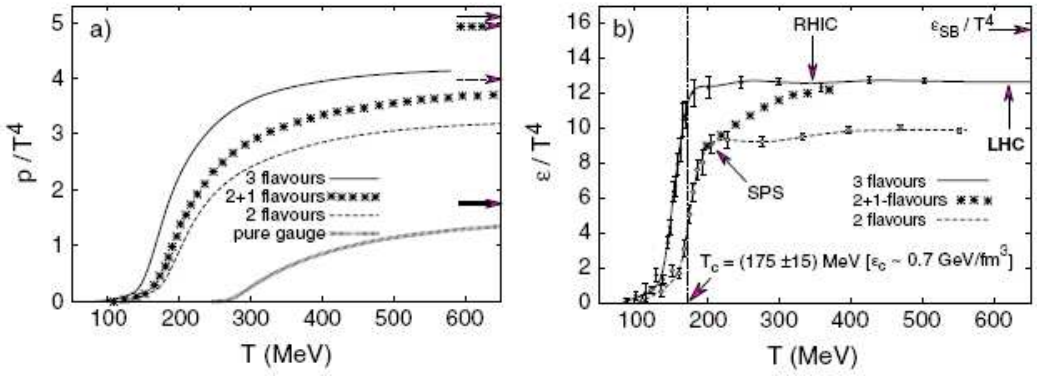

Figure 2: The pressure (a) and energy density (b), in QCD with 0, 2 and 3 degenerate quark flavours as well as with two light (up and down) flavours and a heavier (strange) quark flavour. The arrows on the right-side ordinates show the value of the Stefan-Boltzmann limit for an ideal quark-gluon gas.

The pressure, however, rises more slowly near and above T_c, which indicates that significant non-perturbative effects are to be expected at least up to temperatures $T \simeq (2-3)T_c$. In fact, the observed deviations from the Stefan-Boltzmann limit of an ideal quark-gluon gas are quite significant even at temperatures $T \simeq 5\,T_c$. As seen from the right panel, in ultra-relativistic heavy ion collisions (SPS, RHIC, LHC) one expects to attain energy densities which reach and exceed the critical energy density ε_c, thus making the QCD phase transition feasible in the laboratory conditions.

At the LHC, the critical energy density will be achieved by colliding two lead nuclei at the center of mass energy $\sqrt{s} = 5.5\,\mathrm{TeV}$ per nucleon pair. Different phases of heavy ion collision can be described as follows [5]. Incoming lead nuclei at highly relativistic energies approach each other, subject to the substantial Lorentz contraction relative to their transverse size. Upon initial impact of the nuclei, primordial hard nucleon-nucleon collisions occur. Further reinteractions induce the formation of QGP, whose pressure drives a collective expansion and cooling, followed by hadronization and further expansion in the hadronic phase. The particle abundances and hence the chemical composition of the fireball are frozen almost directly at hadronization, when inelastic processes cease (chemical freeze-out). At thermal freeze-out, the short-range strong interactions cease and the particle spectra are frozen. Since the inelastic cross sections ($\sim 1\,\mathrm{mb}$) are much smaller than the elastic ones ($\sim 100\,\mathrm{mb}$), chemical freeze-out happens significantly before thermal freeze-out is reached.

Thus, the system created in heavy ion collision undergoes a fast dynamical evolution from the extreme initial conditions to the dilute final hadronic state. The objective is then to identify and to assess suitable QGP signatures, allowing to study the properties of QGP.

3 Probes of QGP

The properties of the QGP state can be studied by means of a variety of observables. Mainly, we will be concentrated on particles with the zero longitudinal momentum $p_z = 0$ in the center-of-mass frame of a nucleus-nucleus collision, the so-called midrapidity ($y = 0$) region, where one expects the largest energy deposition of the interpenetrating nuclei. Thus, the main kinematic variable is the transverse momentum p_T of a particle. In ALICE, the QGP observables (probes) are subdivided into three classes: 1) soft probes with the typical momenta $p_T \lesssim 2\,\mathrm{GeV/c}$, 2) heavy-flavour probes, i.e., using the particles having c- and b-quarks, and 3) high-p_T probes in the momentum range about several tens GeV/c. Further each of the classes will be illustrated by a few typical examples.

3.1 Soft Probes of QGP

Charged particle multiplicity. One of the first measurements in the ALICE physics programme will be the charged-particle multiplicity per rapidity unit, or rapidity density, dN_{ch}/dy, determined at midrapidity. The rapidity y is defined according to the equation $y = \frac{1}{2}\ln\frac{E+p_z}{E-p_z}$, E being the energy and p_z being the longitudinal momentum on the direction of the beam axis of a secondary particle in the center-of-mass frame. The use of the rapidity as an independent variable is useful since it changes by an additive constant under the longitudinal Lorentz boosts while the form of the rapidity distribution remains unchanged. Alternatively, one can use the pseudorapidity density $dN_{ch}/d\eta$, $\eta = -\ln\left(\tan\frac{\theta}{2}\right)$ being the pseudorapidity, related to the angle θ between the momentum of a secondary particle and beam axis. The ALICE detector is optimized for the charged-particle density $dN_{ch}/dy = 4000$ and its performance is checked in detailed simulations up to $dN_{ch}/dy = 8000$. Nowadays, the expected value at midrapidity for LHC ranges between 1200 and 2900. The data on the charged particle multiplicity allow one to get the estimate of the energy density that could be reached within the nuclei overlapping zone[6]. Such estimates show that the energy density at LHC is $3-5$ times as many as the one $\varepsilon \approx 15\,\mathrm{GeV/fm^3}$ reached at RHIC.

Hadron yields. Another early measurement of ALICE will be the identified hadron relative abundances. There are several models for the description of hadroproduction. In particular, in the thermal model [7], the interacting system is considered as a grand canonical ensemble of hadrons of various species formed at a chemical freeze-out stage. The model parameters are temperature and barionic chemical potential. This model is very successful for the description of hadroproduction at RHIC energies. Another theoretical model, the statistical hadronization model [8], is based on the assumption that the expected increase of strangeness in ultrarelativistic heavy ion collisions could deviate from the grand canonical description. This deviation is characterized by the strangeness phase space occupancy γ_s and at hadronization $\gamma_s > 1$ (at the LHC, one expects that $\gamma_s > 5$). The data on the multiplicity distribution and relative hadron abundances will allow one to constrain the hadroproduction models.

Particle momentum spectra. Elliptic flow. In the low-p_T regime, the spectra of the most abundantly produced hadrons (π, K, p, Λ, etc.) are well described by the hydrodynamic models of evolution of an exploding fireball [9,10]. In a noncentral collision of two heavy nuclei, the initial nuclear overlap zone is spatially deformed (see Fig. 3, from Ref. [5]). Once the system thermalizes, the pressure gradients along the short axis in the transverse plane are larger than those along the long axis. As a result, hydrodynamic expansion will be stronger along the x-axis relative to the y-axis that leads to the build-up of elliptic flow in the collective matter expansion. The corresponding azimuthal asymmetry in the hadron transverse momentum spectra is characterized by the elliptic flow coefficient v_2, defined by the expansion

$$\frac{d^3N_h}{d^2p_T dy} = \frac{d^2N_h}{\pi dp_T^2 dy}\Big(1 + 2v_2(p_T)\cos 2\varphi + \ldots\Big) \tag{4}$$

(at midrapidity, the system is mirror symmetric in the transverse x-y plane and the odd Fourier harmonics in the azimuthal angle φ are missing). If the matter produced in the reaction zone rescatters efficiently, the spatial anisotropy of the pressure gradients will be transferred into the anisotropy in the momentum distribution. However, if rescattering among the produced particles is weak, an initial period of almost free streaming will reduce the spatial anisotropy and thus reduce the system's ability to convert the spatial anisotropy into the momentum anisotropy. Therefore, a large positive v_2 can only be obtained if the thermalization of the medium is rapid enough. In this way, the elliptic flow coefficient $v_2(p_T)$ serves, in principle, as a quantitative tool for measuring the thermalization time τ_0. According to the RHIC data, the experimentally measured $v_2(p_T)$ for various hadrons (π, K, p, Λ) is best described within the

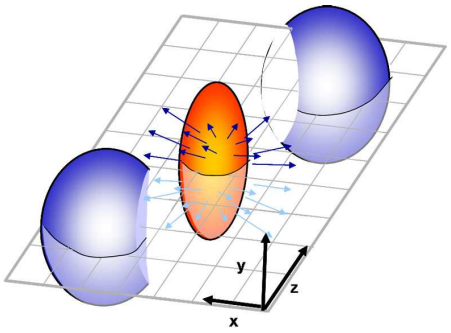

Figure 3: The build-up of elliptic flow in a non-central heavy ion collision.

hydrodynamic approach when implementing a thermalization time of $\tau_0 = 0.5 - 1\,\mathrm{fm/c}$. Besides, for hydrodynamics to build up the observed v_2, the viscosity of the formed medium must remain very small.

3.2 Heavy-flavor probes of QGP

Heavy quarkonia production. Heavy quarkonia of interest include charmonia and bottomonia, where charmonia (bottomonia) are the bound states of the charm (bottom) quark c (b) and antiquark $\bar{c}$ ($\bar{b}$), corresponding to different quantum numbers of a bound state. For specifying the quantum numbers, we use the usual spectroscopic notations, i.e., $^{2S+1}L_J$ with S being the total spin, L total orbital momentum, J total angular momentum of a quark-antiquark pair. Some examples of charmonia states: J/ψ meson (mass $M = 3.097\,\mathrm{GeV}$) - $c\bar{c}$ in the $^3S_1$ state, ψ' meson ($M = 3.685\,\mathrm{GeV}$) - first radial excitation above the lowest lying $^3S_1$ state of $c\bar{c}$, η_c meson ($M = 2.98\,\mathrm{GeV}$) - $c\bar{c}$ in the $^1S_0$ state, χ_{cJ} meson ($M = 3.41, 3.51, 3.56\,\mathrm{GeV}$ at $J = 0, 1, 2$, respectively) - $c\bar{c}$ in the ^3P_J state. Examples of bottomonia states: Υ meson ($M = 9.46\,\mathrm{GeV}$) - $b\bar{b}$ in the $^3S_1$ state, $\Upsilon', \Upsilon'', \Upsilon'''$ (with the masses 10.02, 10.40 and 10.55 GeV, respectively) - three first radial excitations above the ground $^3S_1$ state of $b\bar{b}$.

In nucleus-nucleus collisions, quarkonium suppression is expected to occur due to the Debye screening of the heavy quark interaction in QGP. For example, increase of the energy density reached in the collisions leads to break up of first ψ' and χ_c, and then J/ψ mesons. Further we consider in more detail the suppression of J/ψ mesons, being one of the key probes of the QGP formation in heavy ion collisions[11]. Soon it was realized that besides melting J/ψ mesons in QGP due to the screening of the color charge, there are also a few competing mechanisms which could explain the suppression of J/ψ production in heavy ion collisions. These mechanisms are referred to as cold nuclear matter effects (CNM) and include: 1) absorption of J/ψ by nuclear fragments from colliding nuclei; 2) shadowing of low momentum partons (the depletion of low momentum partons in nucleons bound in nuclei as compared to free nucleons). The last point is important because the gluon fusion is one of the main production mechanisms of J/ψs and the J/ψ yield is therefore sensitive to gluon shadowing. The measurements of the J/ψ yield at CERN SPS at $\sqrt{s} = 17.3\,\mathrm{GeV}$, depicted in the left panel of Fig. 4, show the anomalous suppression beyond the CNM effects in the central collisions when the number of participating nucleons is the largest[12]. This can be considered as a signature of melting of the charmonium states in QGP.

However, measurements of the J/ψ suppression by PHENIX collaboration at RHIC lead to some surprising features. The J/ψ suppression can be characterized by the nuclear modification factor

$$R_{AA}(p_T, y) = \frac{d^2 N^{AA}_{J/\psi}/dp_T dy}{N_{coll} d^2 N^{pp}_{J/\psi}/dp_T dy},$$

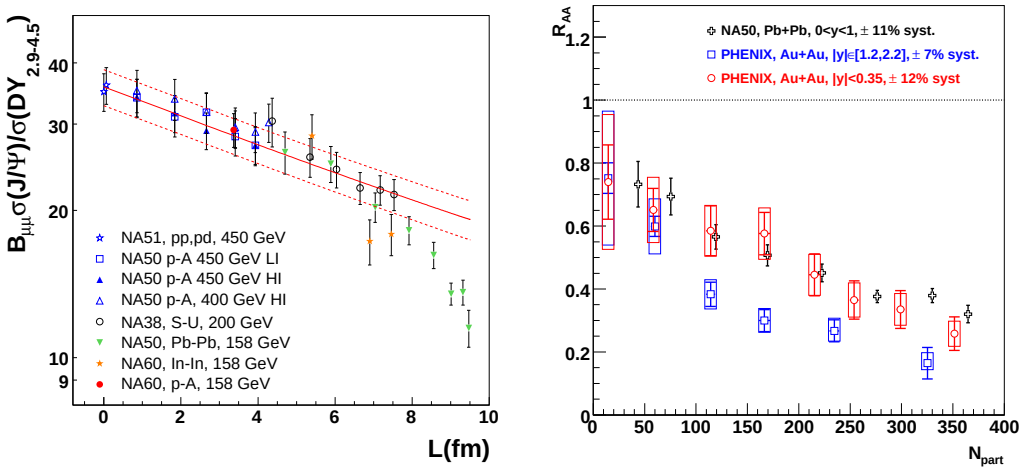

Figure 4: Left: J/ψ yields normalized by Drell-Yan process, as a function of the nuclear thickness L, as measured at the SPS. Right: J/ψ nuclear modification factor for the most energetic SPS (Pb-Pb) and RHIC (Au-Au) collisions, as a function of the number of participants N_{part}.

obtained by normalizing the J/ψ yields in heavy ion collisions by the J/ψ yields in $p+p$ collisions at the same energy times the average number of binary inelastic nucleon-nucleon collisions. This ratio characterizes the impact of the medium on the particle spectrum. If heavy ion collision is a superposition of independent N_{coll} inelastic nucleon-nucleon collisions, then $R_{AA} = 1$, whereas $R_{AA} < 1$ ($R_{AA} > 1$) corresponds to the case of the J/ψ suppression (enhancement). Fig. 4 (right) shows the p_T integrated nuclear modification factor for CERN SPS and RHIC PHENIX experiments [13,14]. There are two surprising results in these measurements. First, the midrapidity suppression (the red boxes) in PHENIX is lower than the forward rapidity suppression (blue boxes) despite the experimental evidence that the energy density is higher at midrapidity than at forward rapidity, and, hence, one could expect that at midrapidity the J/ψs should be more suppressed. Secondly, the nuclear modification factor R_{AA} at midrapidity in PHENIX (red boxes) and SPS (black crosses) are in agreement within error bars although the energy density reached at RHIC is larger than the one reached at SPS.

Possible explanations of these features could be the following [15]. 1. Regeneration of J/ψs in the hot partonic phase from initially uncorrelated c and $\bar{c}$ quarks (quark coalescence model). The underlying idea is that at midrapidity there are more c and $\bar{c}$ quarks to regenerate than at forward rapidity that could explain less suppression of J/ψs at midrapidity. Note that the total number of initial $c\bar{c}$ pairs is larger than 10 in the most central Au+Au collisions at RHIC. 2. J/ψ production could be more suppressed at forward rapidity due to the nuclear shadowing effects. Standard gluon shadowing parametrizations do not tend to produce such an effect but they are poorly constrained by the data and further saturation effects are not excluded.

Thus, the ideal signature of deconfinement would be an onset of the J/ψ suppression. However, such an onset need to be looked at after the CNM effects are properly taken into account. Besides, the role of quark coalescence should be clarified at energies higher than the SPS energy. This is especially important at the LHC because the number of $c\bar{c}$ pairs produced in one central Pb-Pb collision is expected to be larger than 100. One of possible experiments aimed to verify the quark coalescence model is the measurement of the J/ψ elliptic flow. The idea is that if charmonia were produced by coalescence of charm quarks, they should inherit somehow their flow, resulting in a higher v_2 than in the case of the direct production in hard collisions [16].

It is also worth to note that some level of the J/ψ suppression could originate with the reduced feed-down to J/ψ from excited charmonium states (ψ', χ_c), which melt just above the

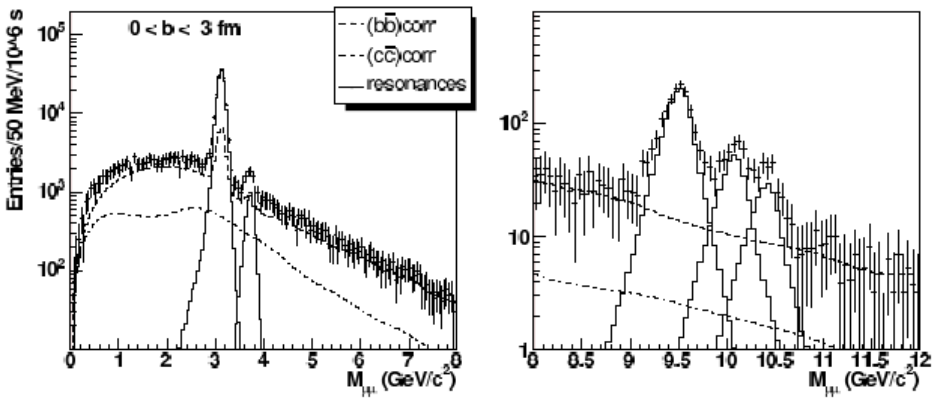

Figure 5: Left: Dimuon invariant mass spectra (after subtraction of the uncorrelated background) in central Pb-Pb collisions for one year of data taking (10^6 s) and luminosity $5 \cdot 10^{26}\,\mathrm{cm}^{-2}\mathrm{s}^{-1}$ in the J/ψ mass region. Right: Same as on the left, but in the Υ mass region.

QGP transition temperature, and from B mesons. Thus, further studies are necessary to make the definite conclusions about the J/ψ production pattern.

Bottomonia are also of a special interest for the studies at the ALICE. One could suppose that bottomonia might be easier to understand than charmonia. Since only about 5 $b\bar{b}$ pairs are expected to be produced in a single central Pb-Pb collision, regeneration should play much less role in the beauty sector at the LHC. Besides, having higher masses, bottomonia originate from higher momentum partons and will less suffer from shadowing effects. These features should ease the separation of the anomalous suppression in the Υ's family.

In ALICE, quarkonia will be detected both in the dielectron channel at midrapidity and in the dimuon channel at forward rapidity. For example, in the dimuon channel, signals of about $7 \cdot 10^5$ J/ψs and 10^4 Υs are expected in the most central Pb-Pb collisions for one year of data taking at nominal luminosity (see Fig. 5 for the corresponding dimuon invariant mass spectra[2]).

Nuclear modification factor for D and B mesons. The heavy-light mesons, $D = (c\bar{q})$, and $B = (b\bar{q})$, are composed of a heavy quark $Q = (c, b)$ and a light antiquark $\bar{q} = (\bar{u}, \bar{d})$. When traversing the dense matter created in nucleus-nucleus collisions, the initially-produced hard partons lose energy mainly on account of medium-induced gluon radiation. Quarks are predicted to lose less energy than gluons which have a higher color charge. The heavy quarks at intermediate p_T will lose less energy as compared with the light quarks at the same momentum, since bremsstrahlung off accelerated heavy quarks is suppressed by a large power of their mass relative to light quarks, $\sim (m_q/m_Q)^4$. Some of heavy quarks will be fragmented into D- and B-mesons. The influence of the medium on their momentum spectrum is characterized by the nuclear modification factor $R_{AA}(p_T)$. Due to the above features, one should observe a pattern of gradually decreasing R_{AA} when going from the mostly gluon-originated light-flavor hadrons ($h^{\pm}$ and π^0) to D and then to B mesons [17]: $R^h_{AA} \lesssim R^D_{AA} \lesssim R^B_{AA}$. The enhancement above the unity of the heavy-to-light ratio $R^{D/h}_{AA} = R^D_{AA}/R^h_{AA}$ probes the color charge dependence of the parton energy loss while the ratio $R^{B/D}_{AA} = R^B_{AA}/R^D_{AA}$ probes the mass dependence of the parton energy loss.

3.3 High-p_T probes of QGP

Jet production. In the high-p_T regime, the mechanism of hadroproduction changes (as compared to the production of hadrons from recombination of partons at p_T up to a few GeV/c). The high-p_T partons produced in the initial stage of a nucleus-nucleus collision undergo multiple scat-

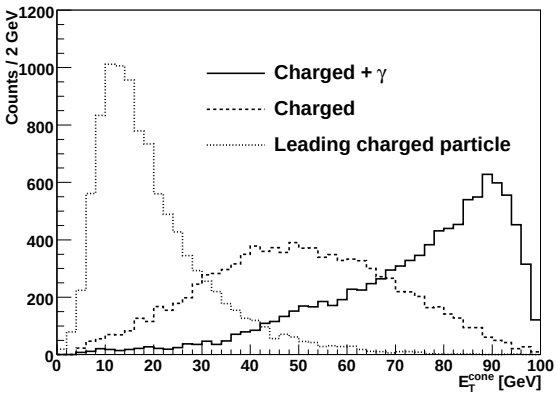

Figure 6: Distribution of reconstructed energy for simulated 100 GeV jets. The results for a charged leading particle, all charged paticles, and all charged particles and photons included in the analysis are shown.

terings inside the collision region and then fragment into a jet, representing a collimated spray of hadrons. These multiple scatterings are expected to induce modifications in the properties of the produced jet, which probe the state of hot and dense matter formed in the initial stage of heavy ion collision. This is the main motivation for studying jet production in nucleus-nucleus collisions. Back-to-back jets are routinely observed in high-energy collisions of elementary particles, but are difficult for identification in the high-multiplicity environment of heavy ion collision. However, a jet typically contains a leading particle which carries most of the momentum of the parent parton. High-p_T spectra in heavy ion collisions thus essentially determine the modification underlying the production of the leading hadron in a jet. This modification can be characterized by the nuclear modification factor $R^h_{AA}(p_T)$ for the leading hadron. RHIC data obtained in central Au+Au collisions show that high-p_T spectra of hadrons are strongly suppressed [18], e.g., for pions, $R^\pi_{AA} \sim 0.2$ up to $p_T \sim 20\,\mathrm{GeV/c}$. These observations provide strong evidence for jet quenching: high-p_T partons lose energy while traversing quark-gluon plasma due to induced gluon radiation and elastic scattering. Note also that at extreme quenching scenarios a full jet reconstruction should provide a better sensitivity to the medium properties. The modification of the jet structure is then expected to be seen in the decrease of the number of particles carrying a high fraction of the jet energy, the increase of the number of the low energy particles and broadening of the distribution of the jet-particle momenta perpendicular to the jet axis.

At the LHC, one anticipates high statistics of jets with the energies at which they can be distinguished from the underlying event. For example, the rate of 100 GeV jets is predicted to be around 10^6 per month in central Pb-Pb collisions. Fig. 6 shows the spectra of the reconstructed jet energy for jets of 100 GeV, using a leading charged particle only, all charged particles, and charged particles plus photons. It illustrates an improvement in the jet energy reconstruction after upgrading ALICE with the Electro-Magnetic Calorimeter (EMCAL) [2].

Direct photons. Direct photons are defined as photons that do not originate from the decay of other particles. Owing to their small electromagnetic coupling, photons once produced do not interact with the surrounding matter and thus probe the state of matter at the time of their production. Early in the collision, the so-called "prompt" photons are produced by hard parton-parton scattering in the primary nucleus-nucleus collisions. They dominate the photon spectrum at $p_T \gtrsim 10\,\mathrm{GeV/c}$. Although their rate decreases as an inverse power of p_T, photons up to several hundred GeV are expected to be detected at LHC. The production cross sections of prompt photons are calculated in perturbative QCD from the basic processes by a convolution with the parton density distribution in the nucleus. The basic processes include the direct

processes such as Compton scattering ($g + q\,(\bar{q}) \rightarrow \gamma + q\,(\bar{q})$) or annihilation ($q\bar{q} \rightarrow \gamma g$), and the bremsstrahlung process in which the photon is produced in the fragmentation of a quark $q \rightarrow \gamma$, or a gluon $g \rightarrow \gamma$. Medium effects in A-A collisions modify the production cross sections of prompt photons as measured in *pp* collisions: nuclear shadowing and in-medium parton energy loss lead to a suppression of the yield, whereas the intrinsic transverse momentum distribution of the partons and medium-induced photon radiation from quark jets enhance the yield. An important background to prompt photon production is the decay $\pi_0 \rightarrow \gamma\gamma$, produced in similar hard partonic processes.

A promising method to probe the medium effects in heavy ion collisions is to use the jets, originating from Compton or annihilation process. Since prompt photons are produced in parton collisions, in which at the central rapidity region the final state photon and parton are emitted almost back-to-back, such jets can be tagged with prompt photons, emitted oppositely to the jet direction. Medium effects then can be identified through the determination of the nuclear modification factor R_{FF} related to the ratio of the fragmentation functions measured in A-A and *pp* collisions and scaled with the number of binary nucleon-nucleon collisions. The fragmentation function of a photon-tagged jet is the distribution of charged hadrons within the jet as a function of p_T/E_γ (E_γ is the photon energy). Medium effects in heavy ion collisions can be also probed by studying photon-hadron and photon-photon correlation functions.

In conclusion, the ALICE experiment at the LHC is aimed to study the physics of strongly interacting matter at extreme energy densities and temperatures, where a new state of matter, quark-gluon plasma, is expected to be reached. Due to its excellent track, vertex-finding and particle-identification capabilities, ALICE will be able to study the properties of QGP by means of a whole set of different and complementary observables.

References

1. ALICE: Physics Performance Report, V. 1. *J. Phys.* G **30**, 1517 (2004).
2. ALICE: Physics Performance Report, V. 2. *J. Phys.* G **32**, 1295 (2006).
3. F. Karsch, *Nucl. Phys.* A **698**, 199 (2002).
4. C. R. Allton et al., *Phys. Rev.* D **66**, 074507 (2002).
5. R. Rapp and H. van Hees, Preprint arxiv: 0803.0901v2.
6. J. D. Bjorken, *Phys. Rev.* D **27**, 140 (1983).
7. A. Andronic, P. Braun-Munzinger, and J. Stachel, *Nucl. Phys.* A **772**, 167 (2006).
8. J. Letessier, and J. Rafelski, *Phys. Rev.* C **73**, 014902 (2006).
9. N. Borghini, and J.-Y. Ollitrault, *Phys. Lett.* B **642**, 227 (2006).
10. M. Chojnacki, W. Florkowski, W. Broniowski, and A. Kisiel, *Phys. Rev.* C **78**, 014905 (2008).
11. T. Matsui and H. Satz, *Phys. Lett.* B **178**, 416 (1986).
12. E. Scomparin (for the NA60 Collaboration), *J. Phys.* G **34**, S463 (2007).
13. B. Alessandro et al., *Eur. Phys. J.* C **39**, 335 (2005).
14. A. Adare et al., *Phys. Rev. Lett.* **98**, 232301 (2007).
15. R. G. de Cassagnac, *J. Phys.* G **35**, 104023 (2008).
16. C. Silvestre (for the PHENIX Collaboration), *J. Phys.* G **35**, 104136 (2008).
17. N. Armesto, A. Dainese, C. A. Salgado, and U. A. Wiedemann, *Phys. Rev.* D **71**, 054027 (2005).
18. K. Reygers (for the PHENIX Collaboration), *J. Phys.* G **35**, 104045 (2008).